ELSEVIER

Materials Science and Engineering A204 (1995) 186–192

MATERIALS SCIENCE & ENGINEERING A

Sonochemical synthesis of nanostructured catalysts

Kenneth S. Suslick*, Taeghwan Hyeon, Mingming Fang, Andrzej A. Cichowlas

School of Chemical Sciences and Materials Research Laboratory, University of Illinois at Urbana-Champaign, 505 S. Mathews Avenue, Urbana, IL 61801, USA

Abstract

Sonochemistry arises from acoustic cavitation; the formation, growth, and collapse of bubbles in a liquid. The implosive collapse of a bubble generates a localized hot spot; a temperature of ~5000 K and pressure of ~1800 atm, with cooling rates that exceed 10^9 K s^{-1}. Using these extreme conditions, we have developed a new synthetic technique for the synthesis of nanostructured inorganic materials. When irradiated with high intensity ultrasound in low volatility solvents under argon, volatile organometallic precursors produce high surface area solids that consist of agglomerates of nanometer clusters. These sonochemically produced nanostructured solids are active heterogeneous catalysts for hydrocarbon reforming and CO hydrogenation. For Fe and Co, nanostructured metals are formed; for Mo and W, metal carbides (e.g., Mo_2C) are produced. Using polymeric ligands (e.g., polyvinylpyrrolidone) or oxide supports (alumina or silica), the initially formed nanoscale clusters can be trapped as colloids or supported catalysts, respectively.

Keywords: Sonochemical synthesis; Nanostructured catalysts

1. Introduction

The preparation of nanostructured materials has been the recent focus of intense study in materials science [1,2]. A variety of chemical and physical preparative methods have been applied to produce materials with nanometer structure, including metal evaporation [3], decomposition of organometallic compounds [4], and the reduction of metal salts [5,6]. Sonochemical decomposition of transition metal carbonyl compounds has also been proven to be a useful technique to generate nanophase transition metals [7,8].

In sonochemical reactions, there is no direct coupling of the ultrasound with chemical species on a molecular level. Instead, the chemical effects of ultrasound originate from transient hot spots formed during acoustic cavitation (the formation, growth and collapse of bubbles in a liquid) [9,10]. The temperature reached during bubble collapse in a cavitating bubble field is approximately 5000 K with a sub-microsecond lifetime [11]. Consequently, acoustic cavitation creates not only extreme temperatures, but also extraordinary cooling rates (above 10^9 K s^{-1}). These exceptional local conditions can be used to generate nanostructured materials.

Sonochemical rates depend on a variety of experimental parameters. In order to achieve good sonochemical yields, precursors should be volatile, since the primary sonochemical reaction site is the vapor inside the cavitating bubbles [12]. In addition, the solvent vapor pressure should be low at the sonication temperature, because the solvent vapor inside the bubble reduces the collapse efficiency.

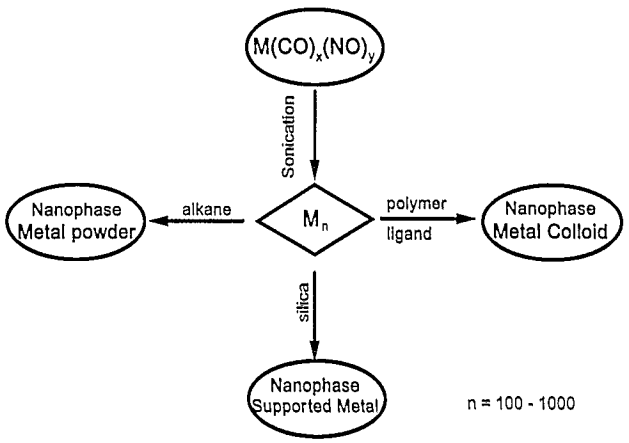

Scheme 1. Sonochemical synthesis of various forms of nanostructured materials.

* Corresponding author.

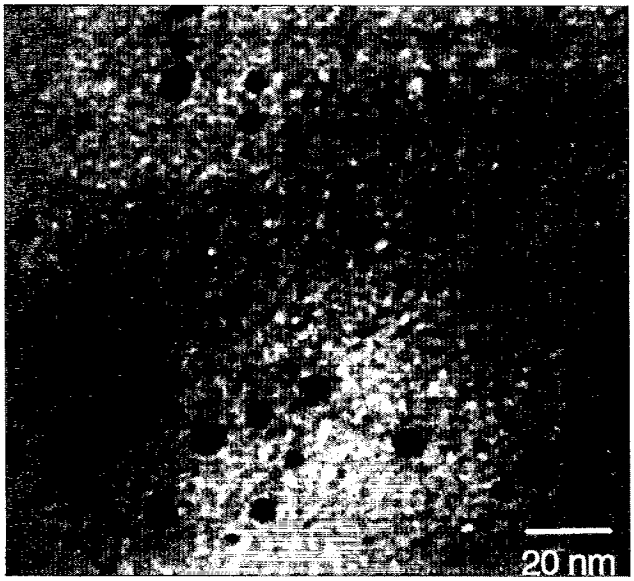

Fig. 1. Transmission electron micrograph of nanostructured Fe–PVP, obtained on a Phillips 420 electron microscope.

The sonochemical synthesis of nanophase materials has the advantage that various classes of materials can be generated simply by changing the reaction medium. When precursors are sonicated in high boiling alkanes such as decane or hexadecane, nanostructured, high porosity metal powders are formed. Using a polymeric ligand (e.g. polyvinylpyrrolidone (PVP)) or inorganic support (silica, alumina, etc.), the initially formed nanometer clusters can be intercepted and nanophase metal colloids and nanostructured supported metal catalysts are respectively synthesized (Scheme 1). A transmission electron micrograph of the nanocolloid Fe–PVP is shown in Fig. 1.

We report here the sonochemical synthesis and heterogeneous catalytic studies of nanostructured Fe on silica, nanostructured Fe–Co alloys and nanostructured Mo_2C catalysts.

2. Experimental details

2.1. General procedures

All manipulations for the preparation of samples were performed using Schlenk vacuum line and inert atmosphere box (Vacuum Atmospheres, < 1 ppm O_2) techniques. Pentane was distilled over sodium benzophenone. Decane and hexadecane were distilled over sodium. Ultrasonic irradiation was accomplished with a high intensity ultrasonic probe (Sonics and Materials, model VC-600, 1 cm Ti horn, 20 kHz, 100 W cm^{-2}).

X-ray powder diffraction data were collected on a Rigaku D-max diffractometer using Cu Kα radiation ($\lambda = 1.5418$ Å). Scanning electron micrographs were taken on a Hitachi S800 electron microscope. Transmission electron micrographs were taken on a Phillips CM-12 electron microscope. Samples for elemental analysis were submitted in sealed vials without exposure to air.

Hydrogen (99.99%, Linde), methane (99.97%, Matheson) and CO (99.0 + %, Linde) were further purified through 5A molecular sieves and oxy-traps (Alltech). Cyclohexane (99 + %, Fischer) was dried over molecular sieves prior to use. In the catalytic reactions with cyclohexane, a MKS mass flow controller maintained the flow of hydrogen at 27.5 cm^3 (STP) min^{-1} to carry the cyclohexane vapor at a constant partial pressure of 0.1 bar through the catalyst. A quartz reactor was used for both adsorption and gas–solid catalytic studies. The catalysts were transferred from an inert atmosphere box to the catalytic rig without exposure to air. Surface areas were calculated by applying the BET equation to the N_2 adsorption isotherm measured at 77 K. The gas products obtained during the temperature-programmed desorption (TPD) and temperature-programmed reaction (TPR) experiments were analyzed by a quadrupole mass spectrometer (Spectra Instruments). The catalytic reaction products were analyzed by gas chromatography (Hewlett-Packard 5730A) on an *n*-octane/Porasil C column with flame ionization detector.

2.2. Synthesis of nanostructured catalysts by sonochemical decomposition

2.2.1. Nanostructured Fe–SiO_2 catalyst

Silica gel (Universal Scientific Inc., 63–100 mesh) was pretreated at 450 °C under vacuum (1×10^{-5} torr) for 10 h before use. To this, a solution of $Fe(CO)_5$ in dry decane was added, and the slurry was irradiated at 20 °C with a high-intensity ultrasonic probe for 3 h under argon. After irradiation, the black powder was filtered and washed with dry pentane in an inert atmosphere box.

Conventional silica-supported crystalline iron catalysts were prepared using the standard incipient wetness impregnation method by dissolving $Fe(NO_3)_3 \cdot 9H_2O$ in an aqueous solution containing silica gel [13]. These samples were dried at 120 °C for 12 h, and calcined at 450 °C under an O_2 flow for 1 h. Reduction of iron supported on silica was carried out in a flow of hydrogen at 200 °C for 1 h, at 300 °C for 1 h, and finally at 450 °C for 2 h.

2.2.2. Nanostructured Fe–Co alloy catalysts

A solution of $Fe(CO)_5$ and $Co(CO)_3(NO)$ in dry decane was irradiated at 0 °C with a high-intensity ultrasonic probe for 3 h under argon. After irradiation, a black powder was formed, which was filtered and washed with dry pentane in the glove box.

2.2.3. Nanostructured molybdenum carbide catalyst

A slurry of molybdenum hexacarbonyl in hexadecane was sonicated at 90 °C for 3 h under argon to yield a black powder. Hexadecane was chosen as a solvent because its vapor pressure is low at the sonication temperature. The powder was filtered inside a dry box, washed several times with purified, degassed pentane.

3. Results and discussion

3.1. Synthesis and catalytic studies of nanostructured silica-supported Fe

Ultrasonic irradiation of decane solutions of iron pentacarbonyl, $Fe(CO)_5$, in the presence of silica gel produces a silica-supported material with nanometer-sized clusters of amorphous iron deposited on the silica surface. The iron loading on the SiO_2 can be easily varied by changing the initial concentration of the $Fe(CO)_5$ solution. Elemental analysis reveals Fe, Si, O and a trace amount of carbon ($< 1\%$) to be present. The origin of carbon most likely arises from the decomposition of CO or the alkane solvent during ultrasonic irradiation.

The amorphous nature of these supported iron particles has been confirmed by several different techniques, including differential scanning calorimetry (DSC), X-ray powder diffraction, and electron-beam microdiffraction. Differential scanning calorimetry shows one exothermic transition at 335 °C corresponding to a disorder–order transition (crystallization) of the amorphous iron. Initial X-ray powder diffraction shows no diffraction peaks; after heat treatment under He at 400 °C (sufficient to induce crystallization) for 4 h, the line characteristic of α-iron metal (d spacings of 2.03, 1.43, 1.17 and 1.04 Å) are observed. After crystallization, the X-ray powder diffraction pattern contains no peaks attributable to iron oxide, iron carbide or other iron-based phases. Electron microdiffraction with a transmission electron microscope confirms these observations and shows only a diffuse ring characteristic of amorphous iron particles.

The transmission electron micrograph showed that the iron particles produced by sonolysis of $Fe(CO)_5$ were highly dispersed on the SiO_2 surface. The iron particles range in size from 3 to 8 nm. Chemisorption of carbon monoxide allowed measurement of the dispersion and the average particle size of the iron supported on the silica surface [14]. CO chemisorption measurement data at -78 °C show the average iron particle size to be ≈ 7.3 nm, which agrees well with TEM data.

The catalytic activity of the silica-supported nanostructured iron was examined for the commercially important Fischer–Tropsch synthesis reaction (i.e., hydrogenation of CO). Fig. 2 compares the activity (in terms of turnover frequency of CO molecules converted per catalytic site per second) of silica-supported nanophase iron and conventional silica-supported iron, prepared by the incipient wetness method, as a function of temperature. These catalytic data were obtained at high iron loading and low dispersion to minimize the effects of support and dispersion. The sonochemically produced iron on silica catalyst is an order of magnitude more active than a comparable conventional supported iron catalyst. Moreover, the silica-supported nanostructured iron catalyst exhibits high activity at low temperatures (< 250 °C), whereas the silica supported conventional iron catalyst has no activity. We hypothesize that the dramatic difference in activity between the two samples below 300 °C may be due to the amorphous nature of iron and the inherently highly-defected surface formed during sonolysis of $Fe(CO)_5$ when the amorphous state of iron is preserved. Above that temperature some decline in activity could be observed, which we believe is due to the iron crystallization process, surface annealing, and deactivation of the catalyst as a result of surface carbon deposition.

Differences between the catalytic properties of the nanostructured iron and of conventional supported catalysts are also observed in selectivities of hydrocarbon synthesis. Under our conditions, the major reaction products for both catalysts are short chain (C_1 to C_4) hydrocarbons and CO_2. Product distribution of hydrocarbons showed that at temperatures lower than 275 °C, the silica-supported nanostructured iron catalyst shows higher selectivity towards long chain hydrocarbons (C_{5+}), whereas the conventional supported iron shows no activity at these temperatures. At temperatures higher than 275 °C (where crystallization can

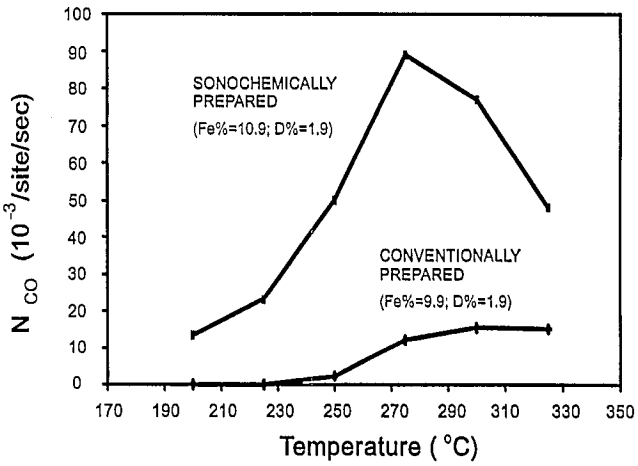

Fig. 2. The catalytic activity of SiO_2 supported amorphous nanostructured iron prepared sonochemically from $Fe(CO)_5$ and SiO_2 slurry (iron loading wt.% = 10.94, and dispersion, $D\% = 1.85$) and SiO_2 supported crystalline iron prepared by the incipient wetness method (Fe wt.% = 9.91, $D\% = 1.86$) as a function of temperature for Fischer–Tropsch synthesis ($H_2/CO = 3.48$, 1 atm, 25 °C).

occur), the reaction product distributions are similar for both types of catalyst.

3.2. Synthesis and catalytic studies of nanostructured Fe–Co alloys

$Fe(CO)_5$ and $Co(CO)_3(NO)$ were chosen as precursors because of their high vapor pressures at modest bulk solution temperatures where they are still thermally stable. The composition of the Fe–Co alloys can be controlled simply by changing the ratio of the vapor pressures (via solution concentrations) of the precursors; alloy compositions ranging from pure Fe to pure Co are readily obtained.

The solid-solution nature of the alloys was confirmed by TEM-EDX results, from multiple locations on the polycrystalline alloy powders. The EDX results show that the alloys are homogeneous on the few-nanometer scale. The original Fe, Co, and Fe–Co alloys produced by ultrasound are amorphous, as determined by XRD, electron-beam microdiffraction, and DSC. After heat treatment under H_2 gas flow at 400 °C for 2 h, all samples underwent crystallization. The XRD results show no peaks attributable to iron/cobalt oxide, iron/cobalt carbide or other iron/cobalt impurity phases. Pure Fe crystallizes to cubic (bcc) structure, pure Co crystallizes to cubic (fcc) and hexagonal (hcp) mixed structures. All the alloys that we have tested so far crystallize in the bcc structure, which is consistent with the known Fe–Co equilibrium phase diagram [15]. Elemental analysis results show that nearly pure metal and alloys are produced (<1% impurity). SEM at high magnification indicates that these materials are porous aggregates of small clusters of 10–20 nm particles, as shown in Fig. 3. Surface electronic structures and surface compositions of the sonochemically prepared Fe–Co alloys were also examined by using X-ray photoelectron spectroscopy (XPS). The XPS measurements were performed on heat treated samples before catalytic reactions. The electronic structures of the surfaces of these samples appear to be the same as the pure metals. The surface compositions of the alloys demonstrate some small enrichment of Fe over Co. Similar trends towards an iron-enriched surface have been reported by other researchers with other preparations using coprecipitation methods [16].

The catalytic studies of the sonochemically prepared Fe–Co alloys were continued on cyclohexane dehydrogenation and hydrogenolysis reactions. All catalysts were treated under H_2 gas flow at 400 °C for 2 h before the catalytic studies. The catalytic activity (in terms of turnover frequency of cyclohexane molecules converted to benzene per surface Fe/Co atom per second) as a function of temperature is shown in Fig. 4. Two kinds of product were formed during the cyclohexane reaction: benzene was the only dehydrogenation reaction

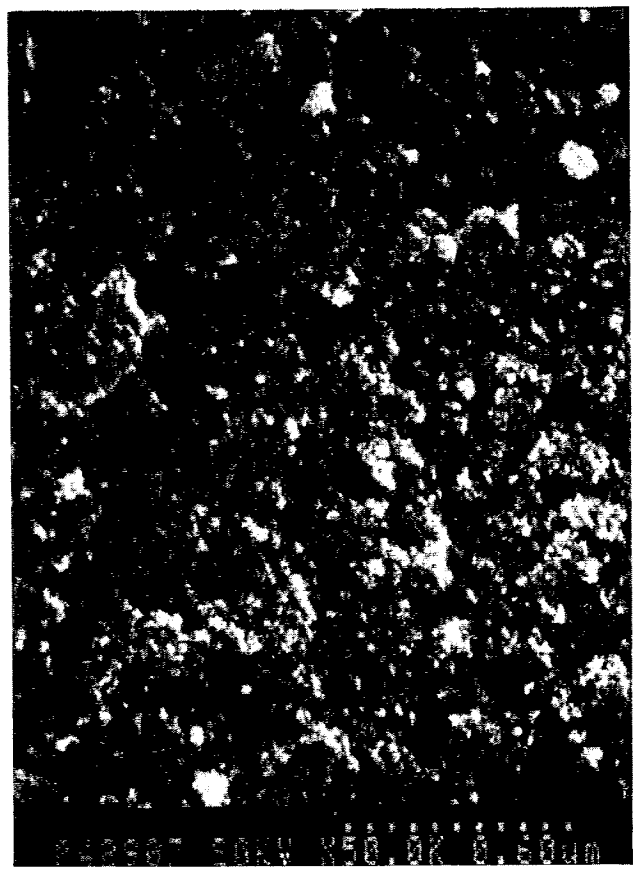

Fig. 3. Scanning electron micrograph of nanostructured 1:1 Fe:Co alloy, obtained on a Hitachi S800 electron microscope.

product and aliphatic hydrocarbons (mostly methane) were the hydrogenolysis reaction products. The catalytic selectivity (in terms of the percentage of benzene among all the reaction products) as a function of temperature is shown in Fig. 5. The catalytic properties of the sonochemically prepared Fe, Co and Fe–Co alloys in the cyclohexane reaction exhibit interesting trends. First, they are all active catalysts for cyclohexane conversion: pure Co has the highest activity (albeit primarily for hydrogenolysis), pure Fe has the lowest activity, and Fe–Co alloys have intermediate activity between pure Fe and pure Co. Second, Fe–Co alloys

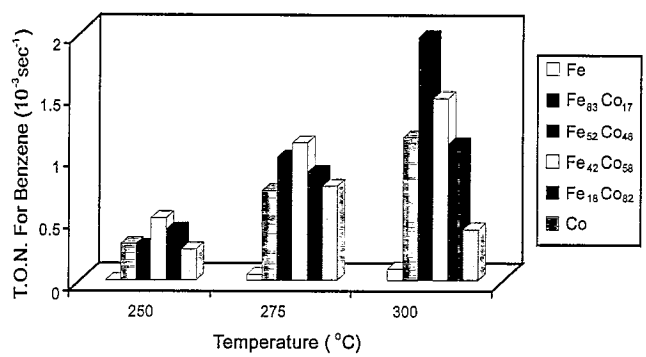

Fig. 4. The catalytic activity of Fe, Co, and Fe–Co alloys for dehydrogenation of cyclohexane to benzene as a function of temperature.

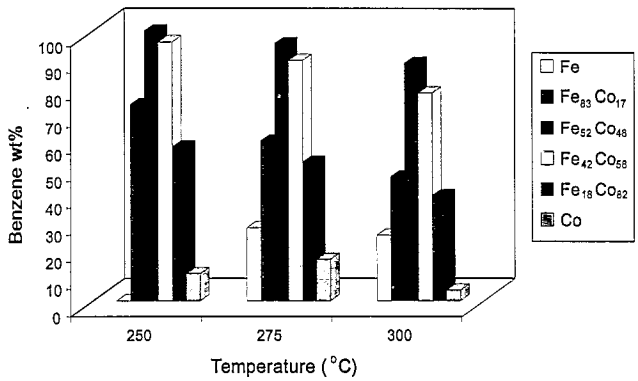

Fig. 5. The catalytic selectivity of Fe, Co, and Fe–Co alloys for dehydrogenation versus hydrogenolysis of cyclohexane as a function of temperature.

generate much more dehydrogenation product (benzene) than pure Fe or Co. Third, the 1:1 Fe–Co alloy has both much higher dehydrogenation activities and selectivities at all reaction temperatures (250 to 300 °C) than the other alloys or pure metals. To our surprise, in the best cases, the selectivity for dehydrogenation approaches 100%. The origin of this high selectivity is currently under further investigation.

3.3. Synthesis and catalytic studies of nanostructured molybdenum carbide

Recently, molybdenum and tungsten carbides have been explored as heterogeneous catalysts because the activity of these carbides is similar to that of the platinum group metals [17–19]. For catalytic applications, high surface area materials are generally needed. The preparation of interstitial carbides of molybdenum and tungsten with high surface areas, however, is very difficult. Boudart and Volpe prepared carbides of molybdenum and tungsten with high surface areas by the temperature programmed carburization of the corresponding nitrides [20]. We present here a simple sonochemical synthesis of nanophase molybdenum carbide from the ultrasonic irradiation of molybdenum hexacarbonyl.

Sonochemical decomposition of molybdenum hexacarbonyl in hexadecane produced a black powder. X-ray powder diffraction (XRD) showed extremely broad peaks centered at a d spacing of 2.4 Å, 1.5 Å and 1.3 Å, which do not match body centered cubic (bcc) lines of molybdenum metal. After the heat treatment at 450 °C under helium flow for 12 h, sharper peaks in the XRD were observed at d spacing values of 2.39 Å, 1.49 Å and 1.27 Å, which match very well with face centered cubic (fcc) molybdenum carbide, Mo_2C (Fig. 6). Elemental analysis also confirmed the stoichiometry of 2Mo/C, but with some oxygen as discussed below. The formation of molybdenum carbide can be explained by the disproportionation of carbon monoxide on the active metal surface to form carbon and carbon dioxide [21].

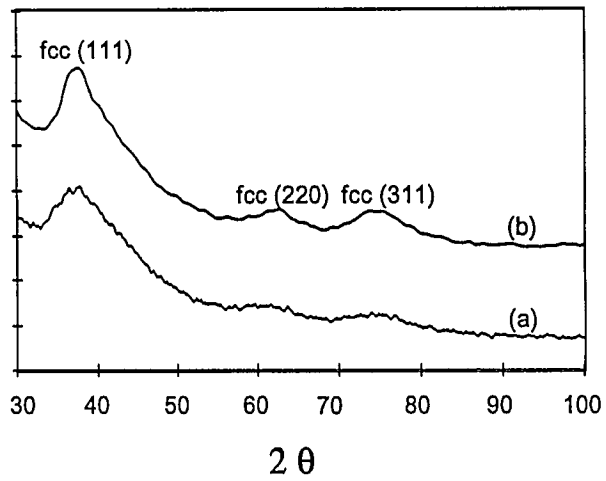

Fig. 6. X-ray powder diffraction patterns of sonochemically produced Mo_2C (a) after synthesis, (b) after heat treatment under He, 450 °C, 12 h.

The SEM showed that the surface is extremely porous. The high resolution TEM showed that the solids were made up of aggregates of 2 nm sized particles (Fig. 7). Consistent with this, the particle size calculated from the line broadening of X-ray powder diffraction was 1.6 nm. Surface area, determined by BET gas adsorption isotherms, was found to be 188 $m^2 g^{-1}$.

Even after heat treatment at 450 °C under helium, the sample still contained about 4 wt.% of oxygen. Since the presence of oxygen could poison the catalytic activity, it was removed before catalytic studies by

Fig. 7. Transmission electron micrograph of sonochemically produced Mo_2C, obtained on a Phillips CM-12 electron microscope.

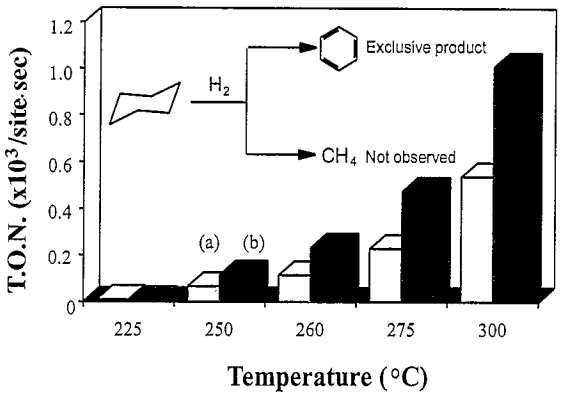

Fig. 8. Catalytic activity of sonochemically produced Mo_2C for dehydrogenation of cyclohexane: (a) sample heat treated under helium at 450 °C for 12 h; and (b) sample heat treated under CH_4/H_2 at 500 °C for 48 h.

heating in a flowing 1:1 CH_4/H_2 mixture at 300 °C for 1 h, then at 400 °C for 1 h, and finally at 500 °C for 48 h. The flow rate of the CH_4/H_2 mixture was 27.5 cm^3 (STP) min^{-1}. After the heat treatment, the elemental analysis results showed the sample was pure Mo_2C; oxygen, excess carbon, and hydrogen had been removed. Electron micrographs showed that the material was still porous and was composed of particles of 3 nm in diameter. The BET surface area decreased slightly to 130 $m^2\ g^{-1}$.

The catalytic activity of the sonochemically produced molybdenum carbide was tested for the dehydrogenation of cyclohexane. Fig. 8 shows the catalytic activity (in terms of turnover frequency of cyclohexane molecules converted per site per second) as a function of temperature for the sample pretreated under CH_4/H_2 at 500 °C for 48 h and for the sample pretreated under helium at 450 °C for 12 h.

At all the reaction temperatures, benzene was the only product formed for either sample. No hydrogenolysis products were detected. Compared to the sample heat treated under CH_4/H_2, the sample heat treated under helium (i.e., with oxide impurity) had the same selectivity (benzene is the only product), but with somewhat lower activity. These results demonstrate that the sonochemically prepared molybdenum carbide is an excellent dehydrogenation catalyst and a rather poor hydrogenolysis catalyst. This is also confirmed by the lack of activity for ethane hydrogenolysis: during 28 h reaction with ethane and H_2 at 300 °C, no methane was detected.

The catalytic properties of Mo_2C (fcc) and Mo_2C (hcp) have been studied intensively in recent years [17–24]. CO hydrogenation, olefin hydrogenation, and hydrocarbon isomerization and hydrogenolysis have been investigated. Few reports, however, mention Mo_2C as an active dehydrogenation catalyst. As a precedent for our studies, carburization of Mo is known to temper Mo metal for dehydrogenation of hydrocarbons [25]. Bell et al. show there is some catalytic activity for ethane hydrogenolysis using Mo_2C (fcc) prepared by reduction and carburization of MoO_3 under similar conditions (300 °C, $H_2/C_2H_6 = 5$) [17]. It seems the sonochemically prepared Mo_2C (fcc) has different and more selective catalytic behavior than the molybdenum carbides generated by the other methods.

4. Conclusions

Sonochemical decomposition of volatile organometallic precursors in high boiling solvents produces nanostructured materials in various forms with high catalytic activities.

Sonication of iron pentacarbonyl with silica in decane at 20 °C generated supported amorphous nanostructured Fe–SiO_2 catalyst. The nanostructured Fe–SiO_2 catalyst showed higher catalytic activity for the Fischer–Tropsch synthesis compared to the conventional Fe–silica catalyst prepared by the incipient wetness method.

Sonochemical decomposition of $Fe(CO)_5$ and $Co(CO)_3(NO)$ in decane at 0 °C generated nanostructured Fe and Co metals and Fe–Co alloys. The sonochemically prepared Fe–Co alloys have large surface areas relative to bulk metal even after heat treatment. We find very high catalytic activity for these Fe, Co, and Fe–Co powders for the dehydrogenation and hydrogenolysis of cyclohexane. The sonochemically prepared Fe–Co alloys show high catalytic activity for the dehydrogenation of cyclohexane to benzene, with 1:1 ratio Fe–Co alloys having selectivities as high as 100%.

Ultrasonic irradiation of molybdenum hexacarbonyl in hexadecane at 90 °C gave nanometer-sized powder of face centered cubic molybdenum carbide. The material was extremely porous with a high surface area and consisted of aggregates of ≈ 2 nm sized particles. The catalytic properties of the sonochemically prepared fcc Mo_2C have been studied on dehydrogenation and hydrogenolysis of cyclohexane and hydrogenolysis of ethane. The catalytic results showed the molybdenum carbide generated by ultrasound is a good dehydrogenation catalyst and a poor hydrogenolysis catalyst.

Acknowledgments

This work was supported by the National Science Foundation. We thank Peggy Mochel, Vania Petrova and the UIUC Center for Microanalysis of Materials, supported by the US Department of Energy, for their assistance in the electron microscopic studies.

References

[1] H. Weller, *Adv. Mater.*, *5* (1993) 88.
[2] G.A. Ozin, *Adv. Mater.*, *4* (1992) 612.

[3] S.C. Davis and K.J. Klabunde, *Chem. Rev.*, *82* (1982) 152.
[4] A.S. Lisitsyn, A.V. Golovin, A.L. Chuvilin, V.L. Kuznetsov, A.V. Romanenko, A.F. Danilyuk and Y.I. Yermakov, *Appl. Catal.*, *55* (1989) 235.
[5] H. Boennemann, W. Brijoux R. Brinkmann and T. Joussen, *Angew. Chem., Int. Ed. Engl.*, *129* (1990) 273.
[6] K.-L. Tsai and J.L. Dye, *J. Am. Chem. Soc.*, *113* (1991) 1650.
[7] K.S. Suslick, S.B. Choe, A.A. Cichowlas and M.W. Grinstaff, *Nature*, *353* (1991) 414.
[8] M.W. Grinstaff, M.B. Salamon and K.S. Suslick, *Phys. Rev. B*, *48* (1993) 269.
[9] K.S. Suslick, *Science*, *247* (1990) 1439.
[10] K.S. Suslick, in K.S. Suslick (ed.), *Ultrasound: Its Chemical, Physical, and Biological Effects*, VCH Press, New York, 1988, p. 123.
[11] E.B. Flint and K.S. Suslick, *Science*, *253* (1991) 1397.
[12] K.S. Suslick, R.E. Cline and D.A. Hammerton, *J. Am. Chem. Soc.*, *106* (1986) 5641.
[13] D. Bianchi, L.M. Tan, S. Borcar and C.O. Bennett, *J. Catal.*, *84* (1983), 358.
[14] J.A. Dumesic, H. Topsøe and M. Boudart, *J. Catal.*, *37* (1975) 513.
[15] T. Nishizawa and K. Ishida, *Bull. Alloy Phase Diagrams*, *5* (1984) 250.
[16] M. Nakamura, B.J. Wood, P.Y. Hou and H. Wise, in *Proc. 4th Int. Cong. on Catal., Tokyo*, Kodansha Ltd., Tokyo, 1981, p. 432.
[17] G.S. Ranhotra, G.W. Haddix, A.T. Bell and J.A. Reimer, *J. Catal.*, *108* (1987) 40.
[18] J.S. Lee, S.T. Oyama and M. Boudart, *J. Catal.*, *125* (1990) 157.
[19] M.J. Ledoux, C. Pham-Huu, J. Guille and H. Dunlop, *J. Catal.*, *134* (1992) 383.
[20] L. Volpe and M. Boudart, *J. Solid State Chem.*, *59* (1985) 332.
[21] N.M. Rodriguez, M.S. Kim and R.T.K. Baker, *J. Catal.*, *144* (1993) 93.
[22] J.S. Lee, L. Volpe, F.H. Ribeiro and M. Boudart, *J. Catal.*, *112* (1988) 44.
[23] G.S. Ranhotra, G.W. Haddix, A.T. Bell and J.A. Reimer, *J. Catal.*, *108* (1987) 24.
[24] C. Pham-Huu, M. Ledoux and J. Guille, *J. Catal.*, *143* (1993) 249.
[25] E.I. Ko and R.J. Madix, *Surf. Sci.*, *100* (1980) L449, L505.